

IRON CARBONATE SCALE GROWTH AND THE EFFECT OF INHIBITION IN CO₂ CORROSION OF MILD STEEL

Kunal Chokshi, Wei Sun, Srdjan Nesic
Institute for Corrosion and Multiphase Technology,
Ohio University
342 West State Street
Athens, Ohio 45701

Abstract

Investigations were conducted to investigate iron carbonate scale precipitation, the interaction between a corrosion inhibition and the precipitating iron carbonate scale, and their effects on the corrosion rate. Both the effects of iron carbonate precipitation on inhibited and uninhibited surfaces and the effects of inhibition on surfaces with iron carbonate scale were studied. The experiments were done in glass cells at 80 °C and a iron carbonate supersaturation range of 7 – 150. A generic imidazoline based inhibitor was added at various points in the iron carbonate scale formation process. Both corrosion rates and precipitation rates were measured using electrochemical and weight gain/loss methods. The scale was later analyzed using scanning electron microscopy (SEM). It was found that the dissolved ferrous ion concentration method, used previously, overestimates the rate of iron carbonate precipitation. Although no antagonism was found under any of other conditions tested, it was seen that the addition of the inhibitor retarded the growth of the iron carbonate scale.

Keywords: iron carbonate, scale, film, inhibitor, precipitation, CO₂ corrosion

Introduction

In CO₂ corrosion, some iron carbide or iron carbonate scale form on the surface due to the corrosion process. As a result, the surface of the metal is not always bare when the inhibitor is applied. Depending on the time when the inhibitor is added, the presence of the corrosion scale could affect the workings of the inhibitor. However very little research has been devoted to study of corrosion inhibition of the steel covered with corrosion product layers.

Gulbrandsen *et al.*, (1998) observed that inhibitor performance was impaired with increasing precorrosion time and increasing temperature. The inhibitor problems were attributed to the presence of the iron carbide layer at the steel surface. The longer the

precorrosion time, the thicker the iron carbide scale would grow and more severely the inhibitor performance was impaired. However, the failure of the inhibitor was not due to transportation of the inhibitor to the metal surface. One reason cited for inhibitor failure was that the high metal dissolution rates prevented the slowly adsorbing inhibitors from adsorbing onto the metal surface and protecting it from corrosion. This phenomenon is described by the electromechanical inhibitor desorption model of Drazic V. and Drazic D. (1990).

Nesic *et al.*, (1995) observed that in the presence of iron carbide as well as iron carbonate scale the performance of an imidazoline-based inhibitor was very poor. They concluded that it was the changes on the steel surface due the precorrosion, which was responsible for the weaker performance of the inhibitor rather than the scale itself acting as a diffusion barrier for the inhibitor. Malik (1995) conducted a study to see the effect of an amine based inhibitor on the surface films. He found that in the presence of iron carbonate scale, lower concentrations of inhibitor seemed to work better than the higher concentrations. He also found that in the presence of inhibitor, there was a transformation of the surface structure of iron carbonate.

Iron carbonate scale growth depends primarily on the kinetics of scale formation. Two different expressions were developed to describe the kinetics of iron carbonate precipitation (respectively by Johnson and Tomson (1991) and Van Hunnik et al. (1996)). The equation given by Johnson and Tomson (1991) was fitted with experimental results at low levels of supersaturation and it overestimated the precipitation rate at large values of supersaturation. Similar results were obtained by the equation developed by van Hunnik et al. (1996). In their experiments, the precipitation rate of iron carbonate was determined by the decrease of ferrous ion concentration in the bulk of the solution. Considering that iron carbonate precipitated not only on the coupons but also elsewhere in the system, measuring precipitation rate by using ferrous ion concentration measurements lead to an overestimation.

From the preceding discussion, it appears that understanding regarding the kinetics of iron carbonate scale precipitation as well as the interaction between the iron carbonate scale and inhibition needs improvement.

Experimental procedure

The experiments were performed in the glass cells. Electrochemical corrosion measurements were performed in the glass cell as shown in Figure 1 by using a potentiostat connected to a PC. Corrosion rates were measured by using the linear polarization resistance (LPR) method. A saturated Ag/AgCl reference electrode used externally was connected to the cell via a Luggin capillary and a porous wooden plug. A concentric platinum ring was used as a counter electrode. Each glass cell was filled with 2 liters of distilled water and 1% wt. NaCl. The solution was heated to 80 °C and purged with 1.0 bar CO₂ gas. After the solution was deoxygenated, the pH was increased from the equilibrium pH 4.18 to the desired pH by adding a deoxygenated sodium bicarbonate

solution. Later the required amounts of Fe^{++} were added in the form of a deoxygenated ferrous chloride salt ($FeCl_2 \cdot 4H_2O$) solution. Then the working electrode was inserted into the solution and the measurements were taken. Prior to immersion, the carbon steel specimen surfaces were polished with 240, 400 and 600 grit SiC paper, rinsed with alcohol and degreased using acetone.

Weight gain/loss measurement was performed in another glass cell shown in Figure 2. Precipitation rate was measured by weight gain/loss method. Precipitation rate of iron carbonate scale was obtained by weighing the coupons which had iron carbonate scale before and after removing the scale. The coupon with the iron carbonate scale on it was observed using Scanning Electron Microscopy (SEM). The chemical composition of the X-65 steel used for all the experiments is shown in Table 1. Two types of generic inhibitors were used for the experiments. The compositions of the inhibitors were shown in Table 2 and Table 3.

Results

The experimental results obtained are presented below in the following manner:

- Experiments with scale formation done at different supersaturations without an inhibitor.
- Experiments done with only inhibitor A and inhibitor B without scale formation.
- Experiments with scale formation done at different supersaturations with addition of inhibitors.

Baseline precipitation experiments at different supersaturations without inhibitor

These set of experiments were designed to see the effect of iron carbonate scale formation at various supersaturations, on both corrosion rate and precipitation rate. The supersaturation was varied from 7 to 150 by changing the pH and the Fe^{++} concentration. The Fe^{++} was added in the system in the form of $FeCl_2 \cdot 4H_2O$ salt solution. Supersaturation of iron carbonate is defined as:

$$SS = \frac{C_{Fe^{2+}} C_{CO_3^{2-}}}{K_{sp}}$$

The effect of change in supersaturation on the corrosion rate is shown in Figure 3. Clearly with higher supersaturation the iron carbonate scale formed faster and the corrosion rate was decreased more rapidly. Error bars display the maximum and minimum values obtained in repeated experiments. Discrepancies in measured precipitation rate were identified when compared to literature correlations which were traced back to the indirect experimental techniques used there to obtain the original precipitation kinetics data (Johnson and Tomson 1991 and Van Hunnik 1996). New data generated in the present project are one to two orders of magnitude lower compared to the calculated results using kinetics expressions given by those authors, as shown in Figure 4. Table 4 shows the conditions under which these supersaturations were obtained. The

supersaturations were varied from a range of 7 to 150 by varying the pH from 6.0 - 6.6 and the Fe^{++} concentration from 10 - 50 ppm. The error bars shown in Figure 4 represent the maximum and the minimum values. Increase in the precipitation rate of iron carbonate is observed in the Figure 4, due to the increase in supersaturation of the solution with respect to iron carbonate. This increase in the precipitation rate, results in a decrease in the corrosion rate of the metal, since the scale blocks a part of the steel surface, prevents it from corroding, and acts as a diffusion barrier for the corroding species as shown in Figure 3.

The top view and the cross-sectional view of the samples at various supersaturations are shown in the Figure 5 - Figure 8. A comparison of scale thickness, crystal grain size, and final corrosion rate for all the baseline experiments at supersaturation of 7 – 150, are shown in Table 5. It is observed that as the supersaturation is increased, the size of the iron carbonate crystal decreases. This is expected since with higher supersaturation and precipitation rates, higher number of crystals nucleates on the surface of the metal. This close proximity of nuclei causes interference in growth of the crystals due to the adjacent crystals. It should be noted that at supersaturation of 7, this phenomenon is not observed since the experiment was stopped after 45 hours and the crystals were not allowed to grow any further.

Baseline experiments done with only inhibitor and without scale

This set of experiments was designed to see the effect of inhibitor concentration on the corrosion rate under non-scaling conditions.

Inhibitor A

The effect of inhibitor A concentration on the corrosion rate is shown in Figure 9. From the figure, it can be seen that at 25 ppm the inhibitor is partially protective, while it decreases the corrosion rate by more than 80% at 50 ppm.

From the potentiodynamic sweeps (Figure 10), the values of the Tafel slopes were measured to be $\beta_a = 62$ mV/decade, $\beta_c = 98$ mV/decade and the 'B' value was calculated to be 16.4 mV. From the sweeps, it can be seen that the inhibitor slows down the anodic reaction as well as the cathodic reaction.

Inhibitor B

The effect of inhibitor B concentration on the corrosion rate is shown in Figure 11. To study the nature of the inhibitor, the potentiodynamic sweeps for the experiments were done at pH 6.60. The sweeps were done in the cathodic direction initially. Then after waiting for sometime for the potential to stabilize the anodic sweep was carried out. From the sweeps (Figure 12), the anodic and the cathodic Tafel slopes for inhibitor B were calculated to be 60 mV/decade and 120 mV/decade respectively and the 'B' value was calculated to be 17.36 mV. Hence, an average value of 17 mV was used for all the experiments.

Inhibitor-scale interactions at supersaturation of 150

In this set of experiments selected concentration of inhibitor A was added to the solution that is at an initial supersaturation of 150 w.r.t. iron carbonate. From Figure 9, it can be seen that at 25 ppm, inhibitor A is partially protective. So, 25 ppm inhibitor was chosen as the concentration to start the testing. In order to study the effect of more protective inhibitor film, 50 ppm inhibitor was added in subsequent experiments.

Simultaneous inhibition and scaling

These experiments were designed to see the interaction of the inhibitor and the iron carbonate scale when both the processes would compete for a place on the metal surface. In the experiment, a supersaturation of 150 was achieved in the beginning of the experiments by adjusting the pH to 6.60 and adding 50 ppm of Fe^{++} . The required amounts of inhibitor A was added after 15 minutes of starting the experiment. On addition of 25 ppm inhibitor A, no effect of addition of the inhibitor was seen on the corrosion rate as well as scale formation, i.e. scale formation dominated the corrosion process.

However, on addition of 50 ppm of inhibitor A, it can be seen that although the corrosion rate drops to 0.2 mm/yr in less than two hours, the final corrosion rate is the same as that without the inhibitor. It can be observed that for this experiment (Figure 13), the inhibitor dominates the iron carbonate scale from the beginning. From the front view of the sample (Figure 14), it can be seen that very little iron carbonate is seen on the surface of the metal. Therefore, it seems that the metal surface is mainly protected due to the presence of the inhibitor and 50 ppm of inhibitor seems to hamper the growth of iron carbonate on the surface of the metal.

Inhibition of a scaled surface

In these set of experiments, the inhibitor was added after 5 hours. These experiments were designed to see the interaction of the inhibitor and the iron carbonate scale when the latter is partially formed. In these experiment, a supersaturation of 150 was achieved in the beginning by adjusting the pH to 6.60 and adding 50 ppm of Fe^{++} . Subsequently, required amounts of inhibitor A was added after 5 hours. It is observed that 25 ppm of inhibitor had no effect on the corrosion rate as well as scale formation.

Figure 15 consists of the experiment in which a supersaturation of 150 was achieved in the beginning, and subsequently 50 ppm inhibitor was added 5 hours after starting the experiment. In this experiment, it can be seen that as soon as the inhibitor is added, the corrosion rate drops rapidly. From the top view of the specimen in Figure 16, it is seen that there are only a few crystals of iron carbonate formed on the surface of the metal. These iron carbonate crystals might have formed before the addition of the inhibitor and subsequently, the inhibitor hampered the growth of the iron carbonate scale.

Inhibitor-scale Interactions at supersaturation of 30

The supersaturation of the solution was lowered to test the inhibitor scale interaction under lower iron carbonate precipitation rates. In this set of experiments, 25 ppm of inhibitor B is added to the solution that is at an initial supersaturation of 30. Since we were in search of a possible antagonistic interaction between the inhibitor and the scale, a concentration of inhibitor that was partially protective was chosen. From Figure 11, it is seen that 25 ppm of inhibitor B fitted our criteria very well.

Simultaneous inhibition and scaling

These experiments were designed to see the interaction of the inhibitor and the iron carbonate scale when both the processes would compete for a place on the metal surface. In the experiment shown in Figure 17, a supersaturation of 30 was achieved in the beginning by adjusting the pH to 6.60 and adding 10 ppm of Fe^{++} . Subsequently 25 ppm inhibitor B was added after 30 minutes. The figure shows the comparison between the experiments with

- Only 25 ppm inhibitor B
- Only iron carbonate scale
- 25 ppm inhibitor added under scaling conditions.

It can be seen that when 25 ppm inhibitor added under scaling conditions, decrease in the corrosion rate is faster than seen in the other two conditions. However, from the logarithmic graph of the above experiment (Figure 18), it is noticed that the final corrosion rate is similar to that without the inhibitor.

From the top view of the sample (Figure 19), it can be seen that very little iron carbonate is seen on the surface of the metal. Therefore, it seems that the metal surface is mainly protected due to the presence of the inhibitor. Adding 25 ppm of inhibitor B seems to hamper the growth of iron carbonate on the surface of the metal.

Inhibition of a scaled surface

In these set of experiments, 25 ppm of inhibitor was added after 35 – 40 hours of starting the experiment that was at an initial supersaturation of 30. Comparison of the experiments with and without inhibitor is shown in Figure 20. It is seen that as soon as the inhibitor is added, the corrosion rate decreases drastically. However, from the logarithmic graph of the same experiment (Figure 21), it is noticed that the final corrosion rate remains similar. From the top and the cross-sectional view of the sample Figure 22, a porous iron carbonate scale of thickness 10 μm is observed.

Inhibitor-scale Interactions at supersaturation of 7

Experiments at supersaturation of 7 were done to test the inhibitor-scale interaction at even slower iron carbonate precipitation rate. In this experiment, the inhibitor was added after creating a very porous iron carbonate scale (Figure 8).

Supersaturation of 7 was achieved in the beginning by adjusting the pH to 6.30 and adding 10 ppm of Fe^{++} . Subsequently, 25 ppm inhibitor B was added after 47 hours. From the comparison of the experiments with and without inhibitor (Figure 23), it is seen that as soon as the inhibitor is added, the corrosion rate decreases and no antagonistic behavior is observed. On observing the scale (Figure 24), it was found that the porosity of the scale was very similar to that of one without inhibitor.

Modeling of inhibitor-scale interaction

From the experimental results it was observed that the protective effects of the corrosion inhibitor and the scale were complementary and no antagonism was observed. However, some interference was seen: the presence of inhibitors hampered the growth of iron carbonate scale. This was initially attributed to the scale inhibition properties of the corrosion inhibitor. Upon a more in-depth analysis it was found that the concentration of Fe^{++} on the surface of the steel could be one of the major factors affecting scale formation. The analysis is explained in the following paragraphs.

In the presence of the inhibitors, the corrosion rate of the metal decreases and the diffusion of Fe^{++} from the bulk solution remains the only source of ions for precipitation at the metal surface. Since, the precipitation of the iron carbonate is much faster than the rate of transportation of Fe^{++} from the bulk of the solution to the surface, the precipitation becomes diffusion-controlled. This leads to slightly more acidic conditions at the metal surface and consequently the supersaturation and the precipitation of iron carbonate decreases.

The above phenomenon can be simulated using Ohio University's MULTICORP V3.0 software package. The model was run under the following conditions: pH 6.60, Fe^{++} concentration of 50 ppm, SS = 150, T = 80 °C. One simulation was run with an inhibitor (assuming 99% efficiency) and another without the inhibitor. It is seen that in the presence of the inhibitor the Fe^{++} concentration (Figure 25) as well as the pH (Figure 26) near the surface of the metal is lower than that in the absence of the inhibitor. This leads to a lower supersaturation and a slower precipitation rate near the metal surface when the inhibitor is added. From the comparison of the scales obtained using the model (Figure 27), it is seen that the thickness of the iron carbonate scale formed in the presence of the inhibitor is approximately five times thinner when compared to the scale thickness formed in the absence of the inhibitor.

Hence, in the absence of corroding conditions at the metal surface, there would be less scale formed at the steel surface. Similar phenomenon was also observed in a series of experiments on stainless steel (Sun, *et al.* 2004). At a supersaturation of 30, it was found that even after 3 days no iron carbonate scale was formed on the surface of steel. In an experiment done at supersaturation of 150, scale precipitated on stainless steel was approximately 50% of that compared to corroding mild steel.

From the above analysis, it is deduced that the concentration of Fe^{++} at the metal surface might be the primary reason the growth of scale is hampered in the presence of inhibitor. In addition, this could also be in part due to the scale inhibition properties of the inhibitor.

Conclusions

Iron carbonate scale precipitation and the interaction between the inhibitor film and the iron carbonate scale have been studied under scaling conditions. The interaction was tested using various concentrations of two imidazoline-based generic inhibitors in the iron carbonate supersaturation range of 7 – 150. Based on the experimental conditions, the main research findings are:

- The weight gain/loss method is a more reliable method for obtaining the precipitation rate than the previously used techniques involving ferrous ion concentration method. The calculated results obtained by previous kinetics expressions using the traditional dissolved ferrous ion concentration method overestimate the precipitation rate.
- The generic corrosion inhibitors used in this study work by slowing down anodic as well as cathodic reactions.
- Above a certain threshold concentration, both inhibitors hamper the growth of the iron carbonate scale. This could be a result of a decreased concentration of Fe^{++} at the surface of the steel and/or scale inhibition properties of the corrosion inhibitor.
- No conditions were found under which inhibitor and scale interacts in an antagonistic manner. i.e. in all of the conditions investigated, the combination of inhibitor and iron carbonate scale never failed to reduce the corrosion rate.

References

1. Gulbrandsen E., S. Nestic, A. Stangeland, T Buchardt, B. Sundfaer, S. M. Hesjevik, S. Skjerve “Effect of precorrosion on the performance of inhibitors for CO_2 corrosion of carbon steel,” CORROSION/1998, paper no. 013, (Houston, TX: NACE International, 1998).
2. V. J. Drazic and D. M. Drazic, “Influence of the metal dissolution rate on the Anion and inhibitor adsorption”, Proc. 7th European Symposium on Corrosion Inhibitors (7SEIC): Ann. Univ. Ferrara, N.S., Sez. V, Suppl. N. 9, 1990 (Ferrara, 1990), p.99.
3. Nestic S., W. Wilhelmsen, S. Skjerve and S. M. Hesjevik “Testing of inhibitors for carbon dioxide corrosion using the electrochemical techniques,” Proceedings of the 8th European Symposium on Corrosion Inhibitors, Ann. Univ. Ferrara, N.S., Sez. V, Suppl. N. 10, (1995): p.1163.
4. Malik H., “Influence of C16 Quaternary amine on surface films and polarization resistance of mild steel in carbon dioxide saturated 5% sodium chloride,” Corrosion, Vol.51 (1995): p.321.
5. Johnson, M. L., & Tomson, M. B. (1991). Ferrous carbonate precipitation kinetics and its impact CO_2 corrosion. *Corrosion/91*, Paper No. 268, NACE International, Houston, Texas.

6. van Hunnik, E. W. J., & Hendriksen, E. L. J. A. (1996). The formation of protective FeCO₃ corrosion product layers. *Corrosion/96*, Paper No. 6, NACE International, Houston, Texas.
7. Sun, W., Chokshi, K., Nestic, S., & D. Gulino (2004). A study of protective iron carbonate scale formation in CO₂ corrosion, AIChE, Austin, Texas.

Tables

Table 1. Chemical Composition of X65 (wt.%) (Fe is in balance)

Al	As	B	C	Ca	Co	Cr	Cu	Mn	Mo	Nb
0.0032	0.005	0.0003	0.050	0.004	0.006	0.042	0.019	1.32	0.031	0.046
Ni	P	Pb	S	Sb	Si	Sn	Ta	Ti	V	Zr
0.039	0.013	0.020	0.002	0.011	0.31	0.001	0.007	0.002	0.055	0.003

Table 2. Formulation of inhibitor A

Compound	Composition (by weight)
Isopropyl alcohol	35%
Water	35%
Imidazoline acetate salts	30% (1:1 DETA/Tall oil imidazoline neutralized to pH 5.0)

Table 3. Formulation of inhibitor B

Compound	Composition (by weight)
Methanol	25%
Water	25%
Imidazoline acetate salts	25% (1:1 DETA/Tall oil imidazoline neutralized to pH 5.0)
Benzyl dimethyl coco-quat chloride	25%

Table 4. Bulk supersaturation of the solution at various pH and Fe⁺⁺ concentration

pH	Fe ⁺⁺ Concentration/ ppm	Supersaturation
6.00	50	9
6.30	10	7
6.30	50	37
6.60	10	30
6.60	50	150

Table 5. Summary of baseline experiments at supersaturation 7 – 150, T = 80 °C, no inhibitor, stagnant solutions

SS	Experimental time/ hr.	Scale thickness / μm .	Crystal grain size / μm .	Final corrosion rate / mm/yr.
7	45	10	10	0.65
9	19	No scale	No scale	1.8
30	85	30 – 40	15 - 25	0.027
37	87	30 - 40	15 - 25	0.13
150	19	15 - 25	5	0.1

Figures

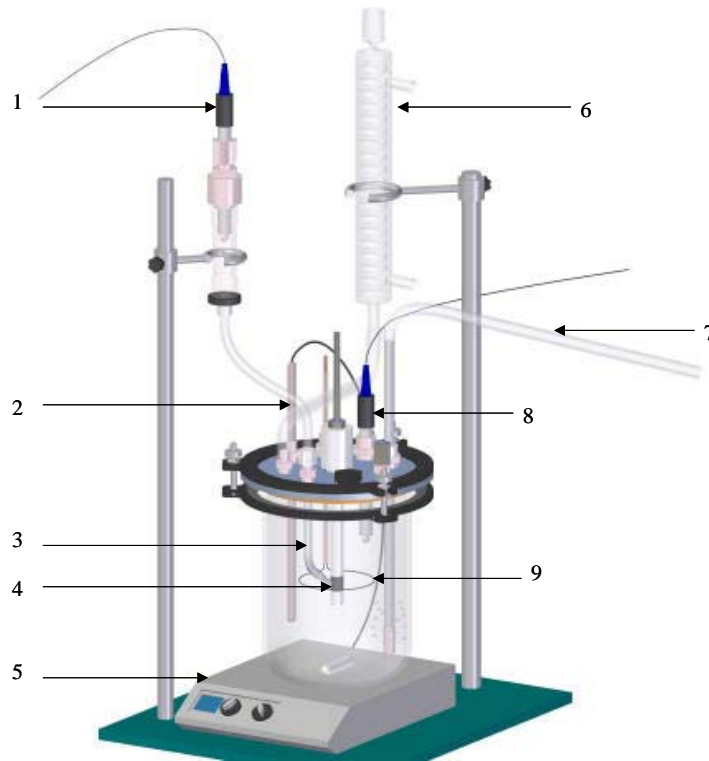


Figure 1. Schematic of a glass cell used for electrochemical measurements: 1. Reference electrode; 2. Temperature probe; 3. Luggin capillary; 4. Working electrode; 5. Hot plate; 6. Condenser; 7. Bubbler for gas; 8. pH electrode; 9. Counter electrode

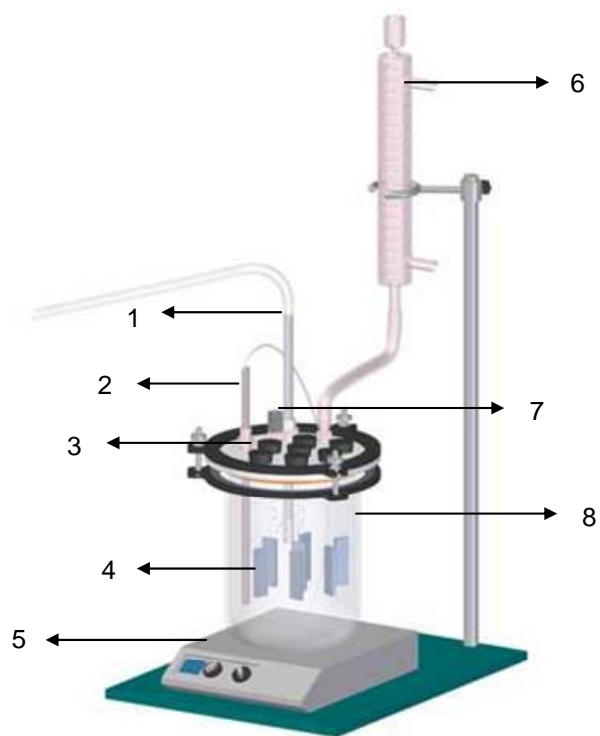


Figure 2. Schematic of a glass cell used for weight gain/loss method: 1. bubbler; 2. temperature probe; 3. rubber cork with nylon cord; 4. steel coupon; 5. hot plate; 6. condenser; 7. pH probe; 8. glass cell.

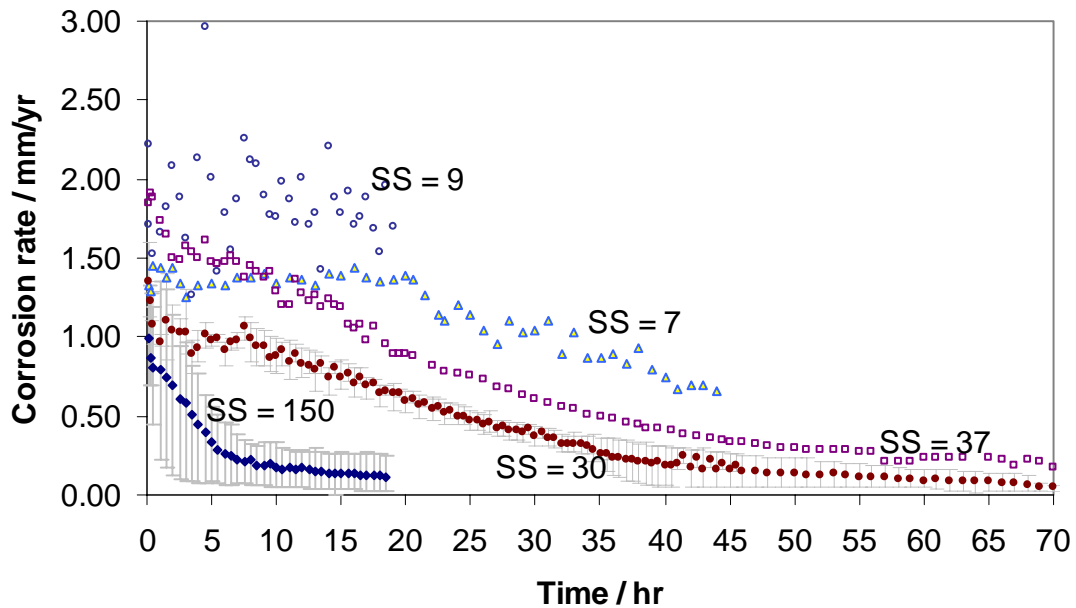


Figure 3. Effect of supersaturation SS on corrosion rate at $T = 80\text{ }^{\circ}\text{C}$, no inhibitor, stagnant conditions. Error bars represent minimum and maximum values obtained in repeated experiments.

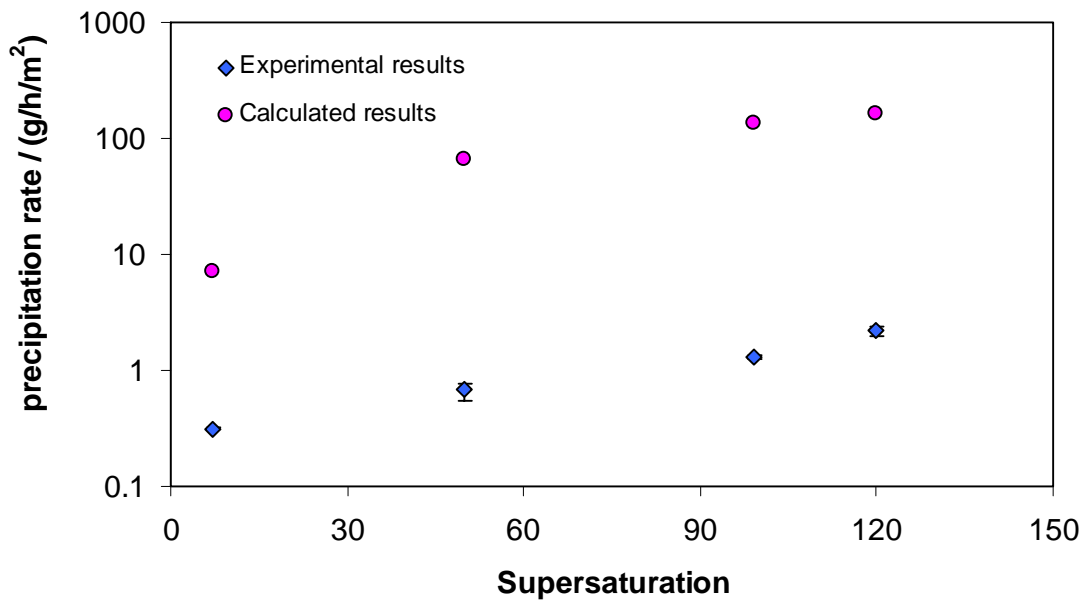


Figure 4. Both experimental and calculated (by using kinetics expression given by van Hunnik, 1996) precipitation rates of iron carbonate under supersaturations of 7 to 150 at a temperature of $80\text{ }^{\circ}\text{C}$.

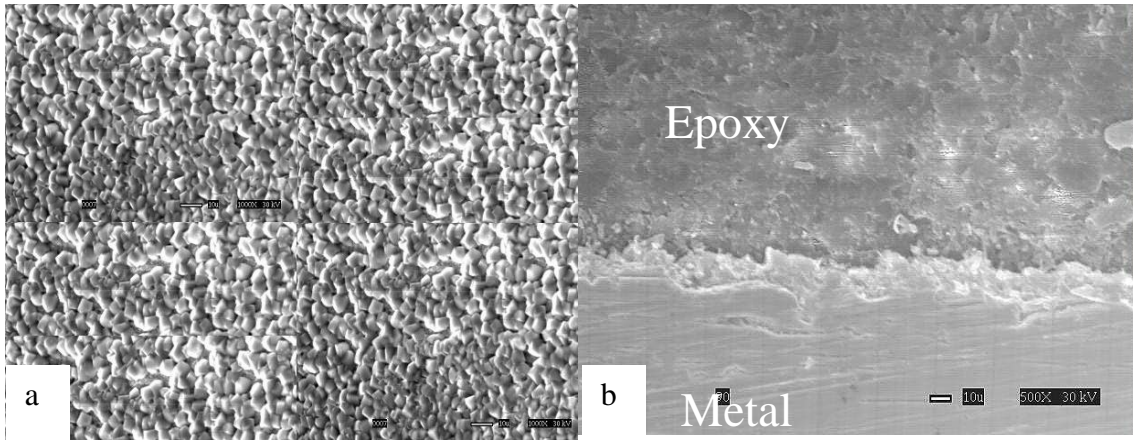


Figure 5. The top view (a) and the cross-sectional view (b) of the sample at 500X, for pH 6.60, $Fe^{++} = 50$ ppm, no inhibitor, SS = 150, $T = 80$ °C, stagnant conditions.

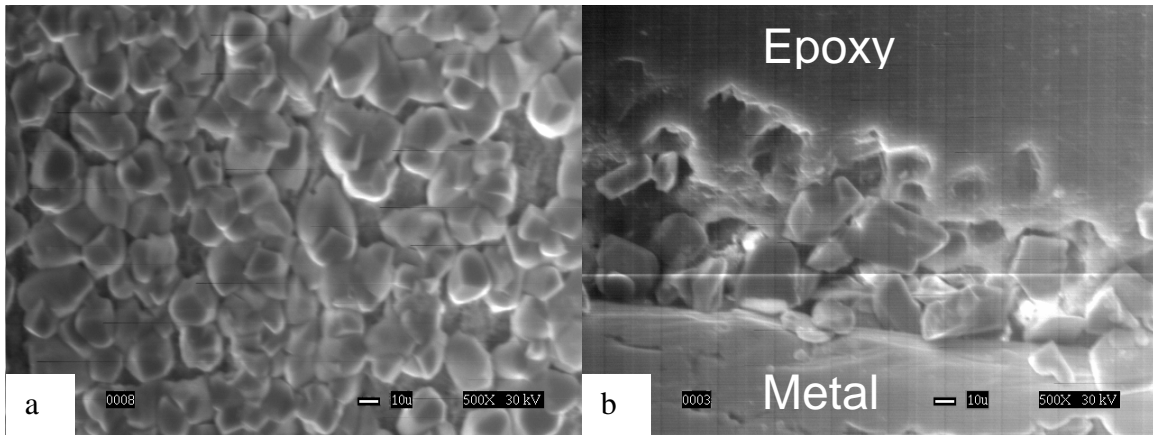


Figure 6. The top view (a) and the cross-sectional view (b) of the sample at 500X, for pH 6.60, $Fe^{++} = 10$ ppm, no inhibitor, SS = 30, $T = 80$ °C, stagnant conditions.

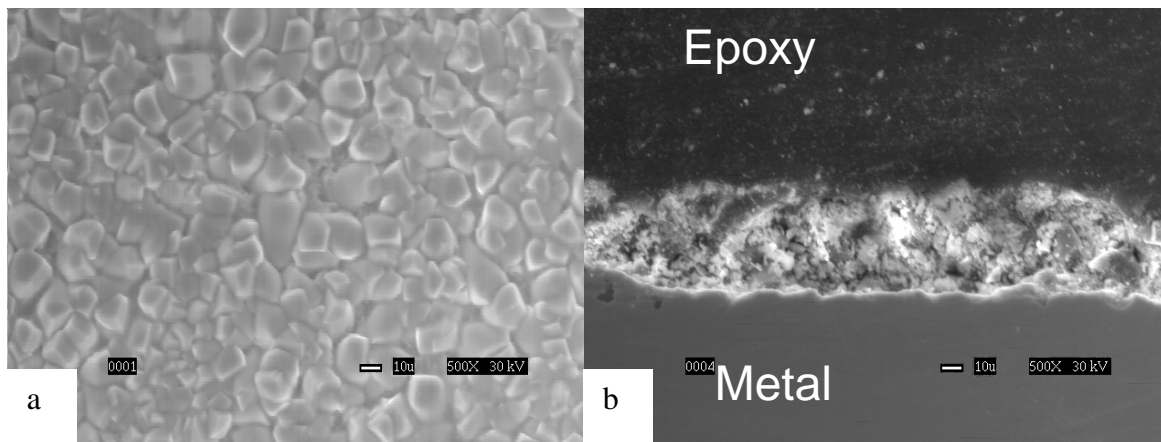


Figure 7. The top view (a) and the cross-sectional view (b) of the sample at 500X, for pH 6.30, $Fe^{++} = 50$ ppm, SS = 37, $T = 80$ °C, no inhibitor, stagnant conditions.

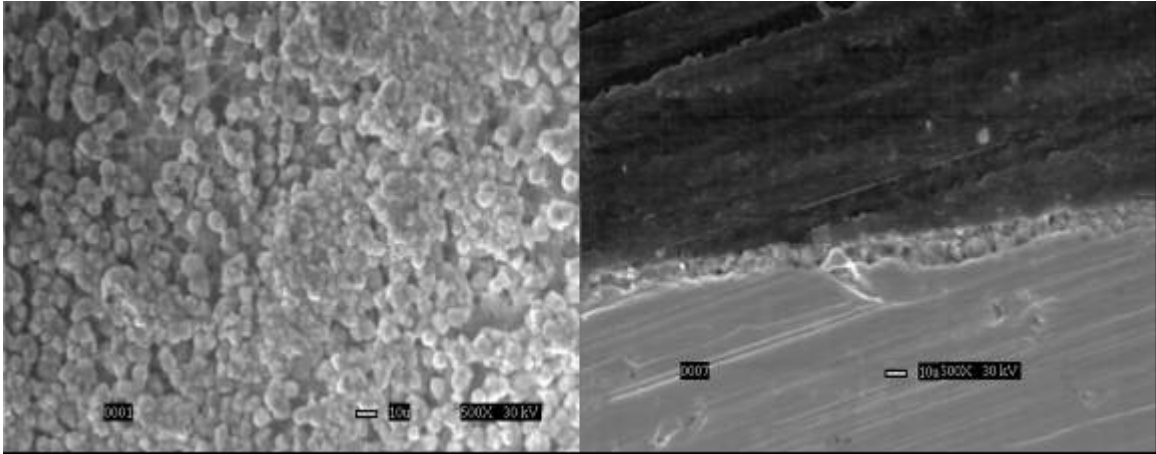


Figure 8. The top view (a) and the cross-sectional view (b) of the sample at 500X, for pH 6.30, $\text{Fe}^{++} = 10$ ppm, SS = 7, T = 80 °C, no inhibitor, stagnant conditions.

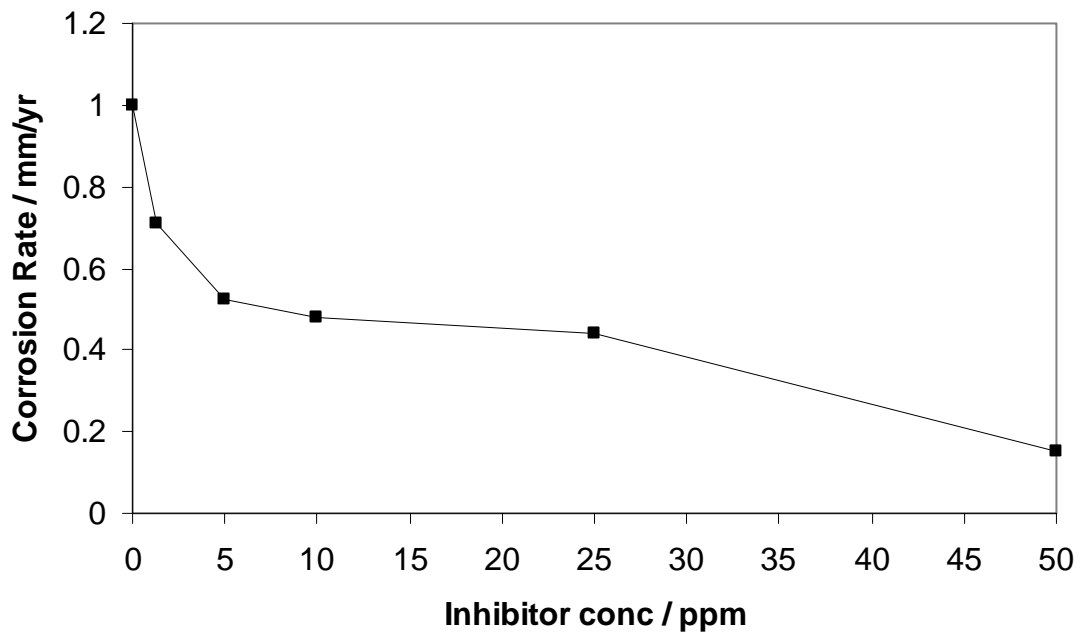


Figure 9. Effect of inhibitor A concentration on the corrosion rate for pH 6.6, T = 80 °C, no Fe^{++} added, stagnant conditions.

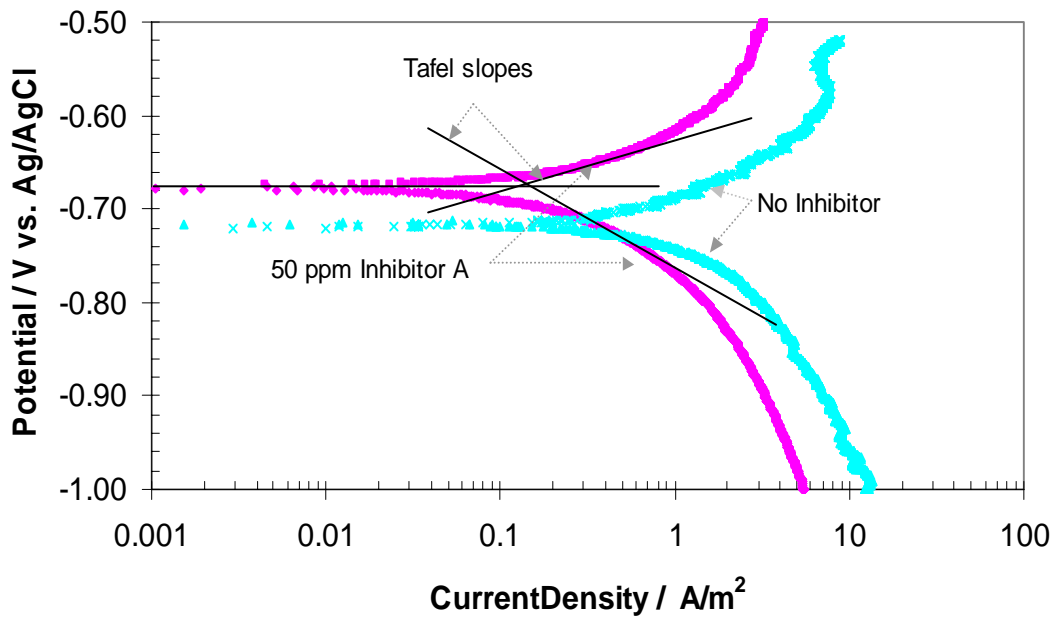


Figure 10. Polarization curves for 50 ppm inhibitor A at pH 6.6, $T = 80\text{ }^{\circ}\text{C}$, no Fe^{++} added, stagnant conditions.

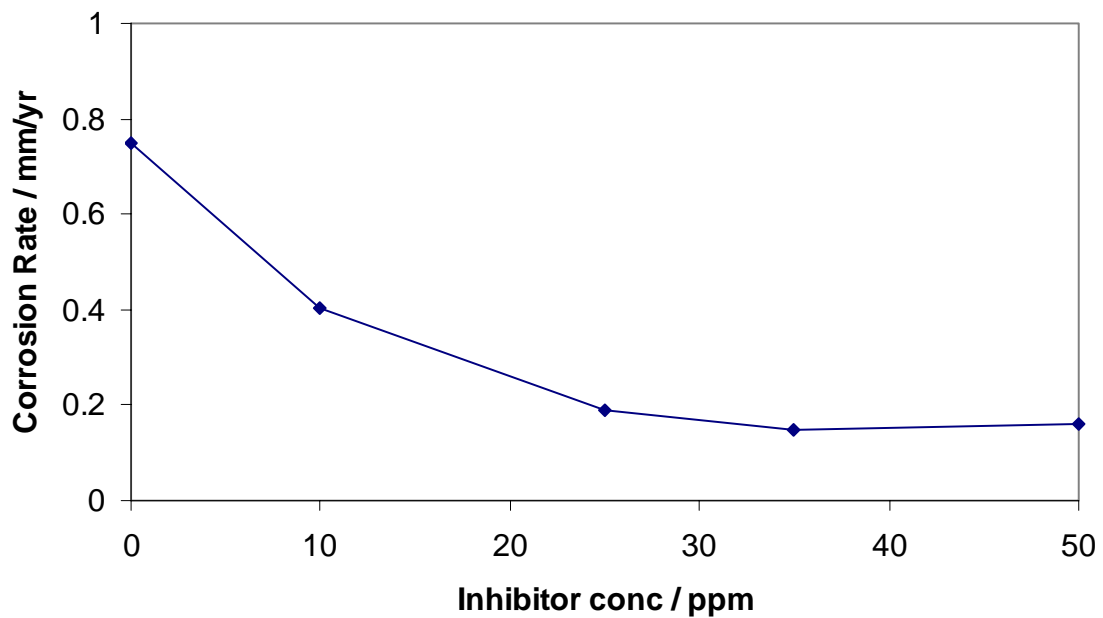


Figure 11. Effect of inhibitor B concentration on the corrosion rate between pH 6.0-6.6, $T = 80\text{ }^{\circ}\text{C}$, no Fe^{++} added, stagnant conditions.

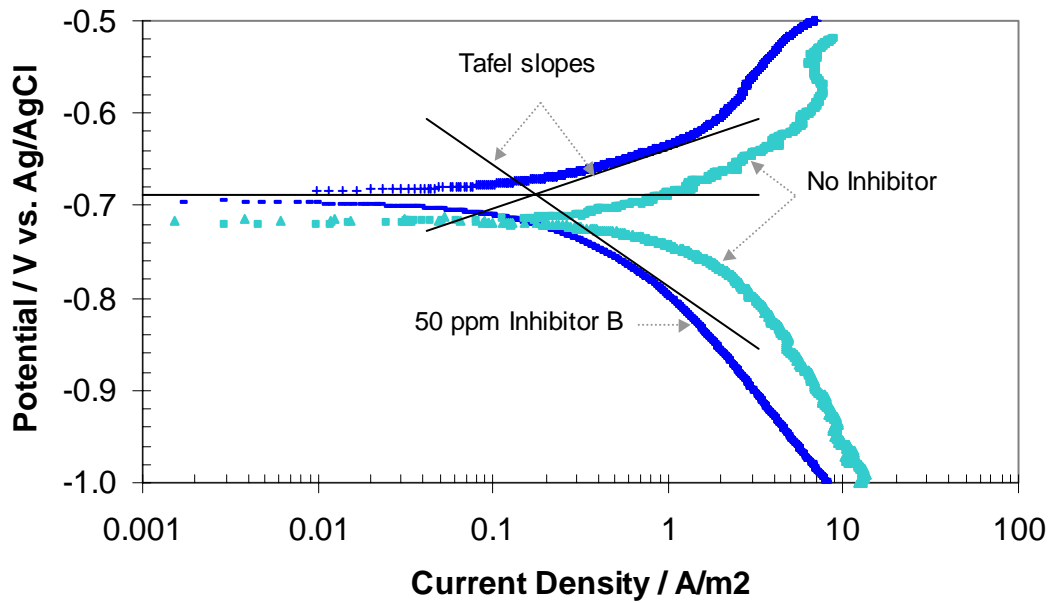


Figure 12. Polarization curves for 50 ppm inhibitor B showing the tafel slopes, at pH 6.6, T = 80 °C, no Fe⁺⁺ added, stagnant conditions.

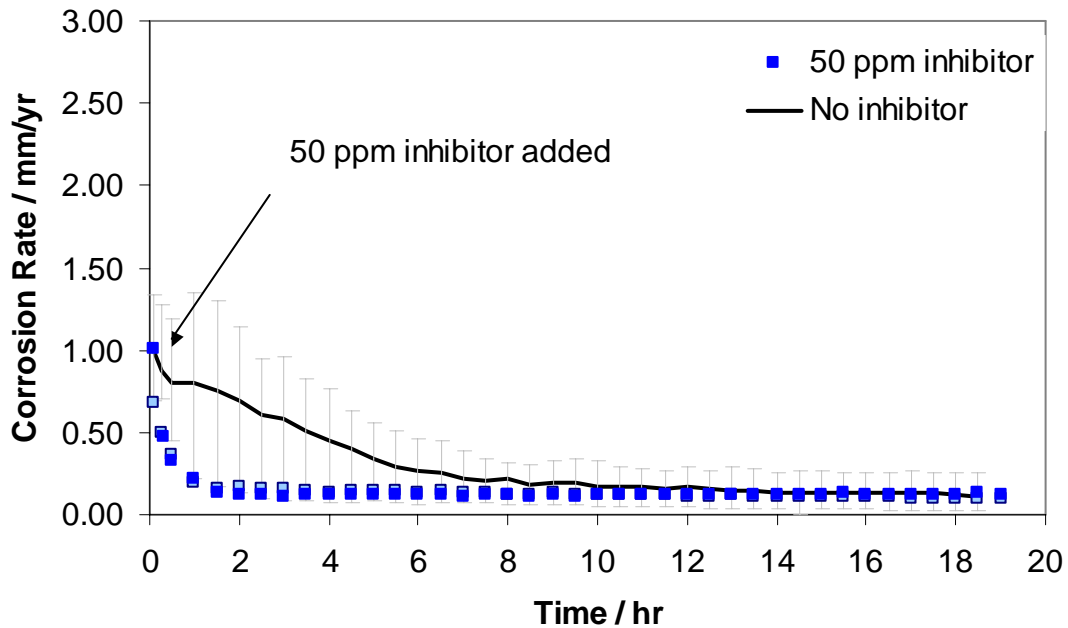


Figure 13. Effect of addition of 50 ppm inhibitor A (added initially) on the corrosion rate for pH 6.60, Fe⁺⁺ = 50 ppm, SS = 150, T = 80 °C, stagnant conditions. Error bars represent minimum and maximum values obtained in repeated experiments. (For an SEM image of a coupon used in this experiment see Figure 14).

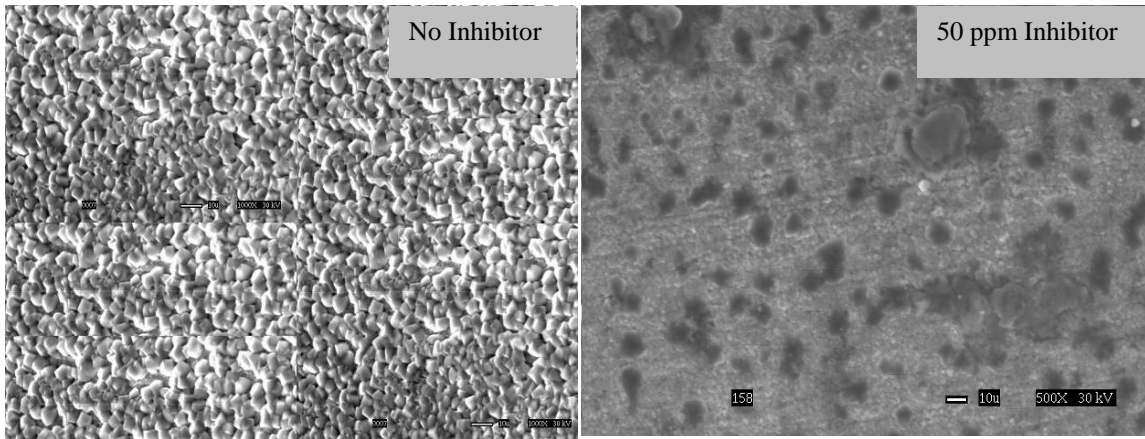


Figure 14. Comparison of top view for specimen at 500X with 50 ppm inhibitor A and without inhibitor at pH 6.60, $\text{Fe}^{++} = 50$ ppm, SS = 150, $T = 80$ °C , stagnant conditions. (For the corrosion rate see Figure 13.)

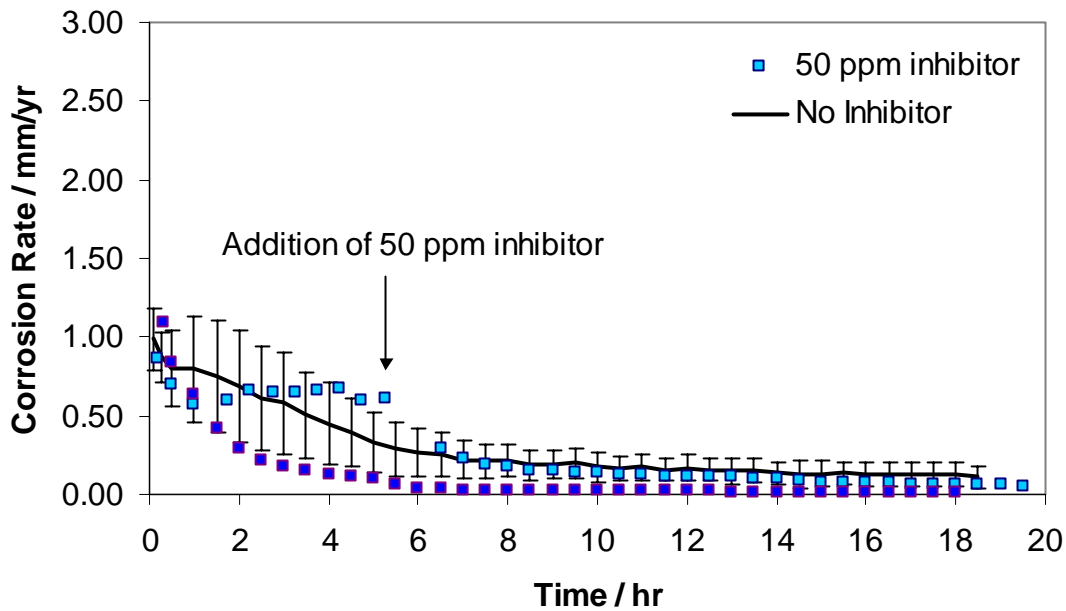


Figure 15. Effect of addition of 50 ppm inhibitor A after 5 hours on corrosion rate for pH 6.60, $\text{Fe}^{++} = 50$ ppm, SS = 150, $T = 80$ °C, stagnant conditions. (For an SEM image of a coupon used in this experiment see Figure 16).

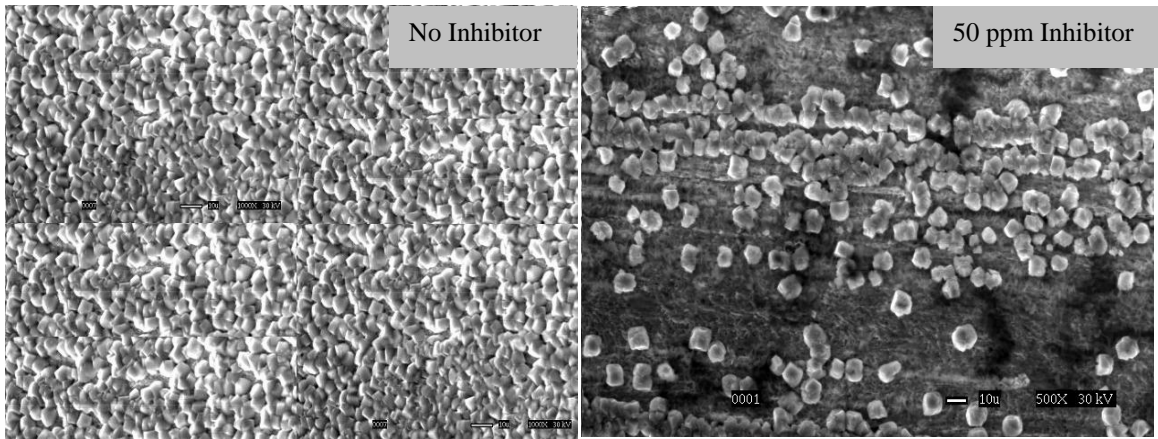


Figure 16. Comparison of top view for specimen at 500X with 50 ppm inhibitor A added after 5 hours and without inhibitor at pH 6.60, $Fe^{++} = 50$ ppm, SS = 150, T = 80 °C, stagnant conditions. (For the corrosion rate see Figure 15.)

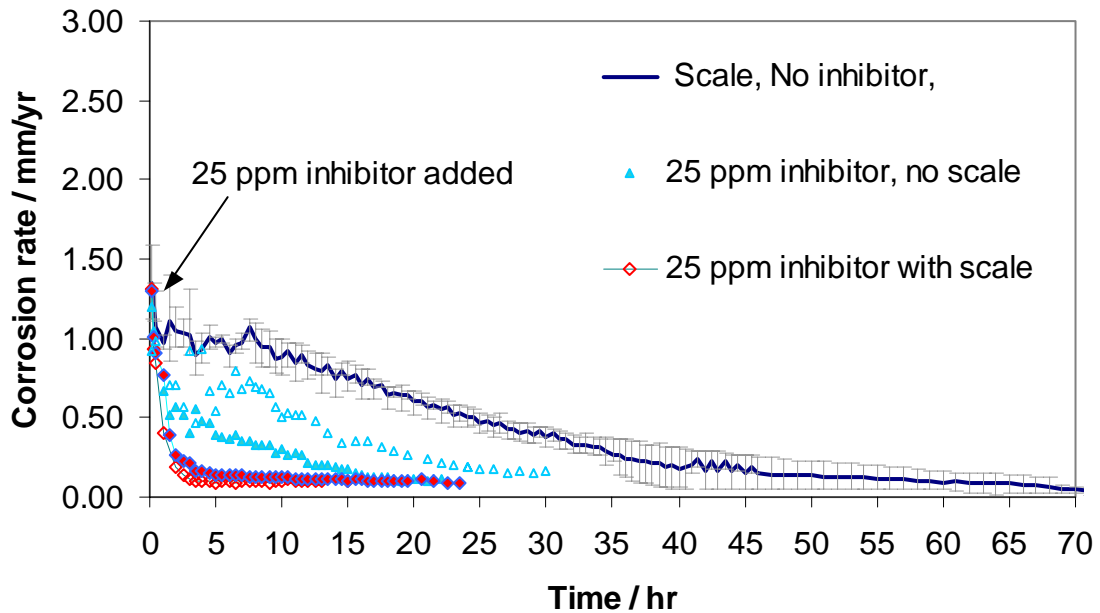


Figure 17. Effect of addition of 25 ppm inhibitor B added after 0.5 hr. on corrosion rate for pH 6.60, $Fe^{++} = 10$ ppm, SS = 30, T = 80 °C, stagnant conditions. Same symbol shapes depict repetitions of the same experiments. Error bars represent minimum and maximum values obtained in repeated experiments.

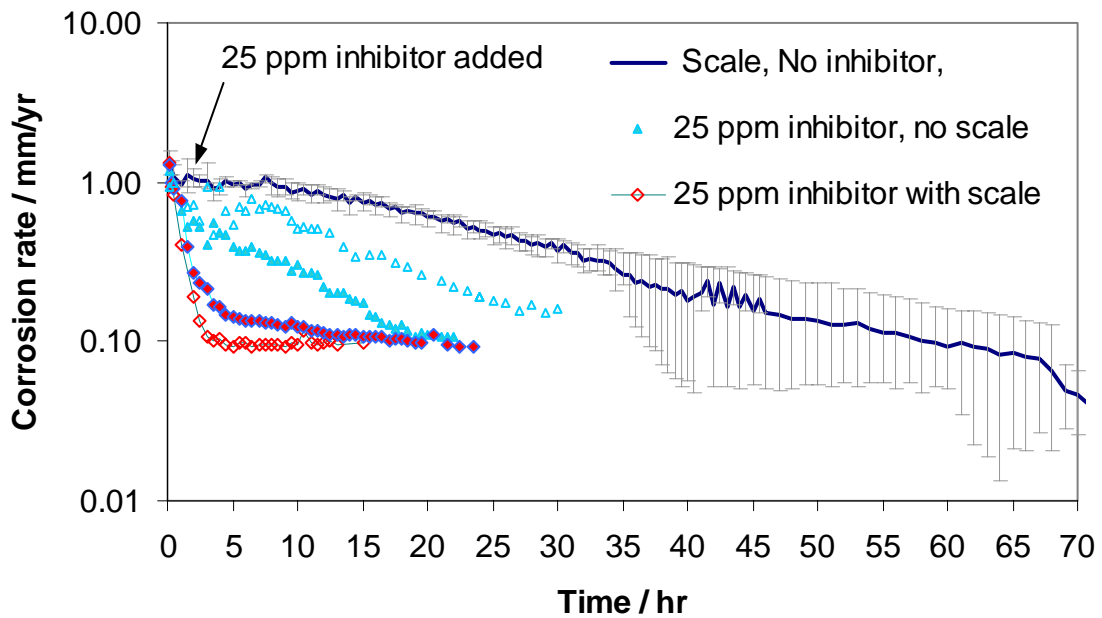


Figure 18. Effect of addition of 25 ppm inhibitor B added after 0.5 hr. on corrosion rate for pH 6.60, $Fe^{++} = 10$ ppm, SS = 30, $T = 80$ °C, stagnant conditions. Same symbol shapes depict repetitions of the same experiments. Error bars represent minimum and maximum values obtained in repeated experiments. For an SEM image of the coupon used in this experiment see Figure 19.

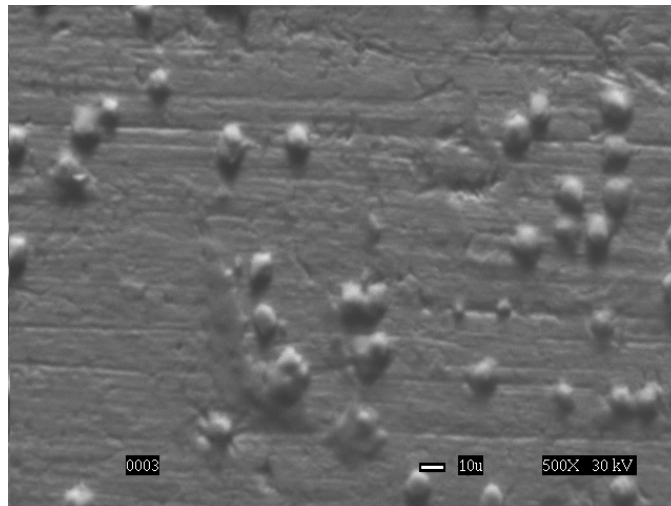


Figure 19. The top view of sample at 500X when 25 ppm inhibitor B is added after 0.5 hr for pH 6.60, $Fe^{++} = 10$ ppm, SS = 30, $T = 80$ °C, stagnant conditions. (For the corrosion rate see Figure 18.)

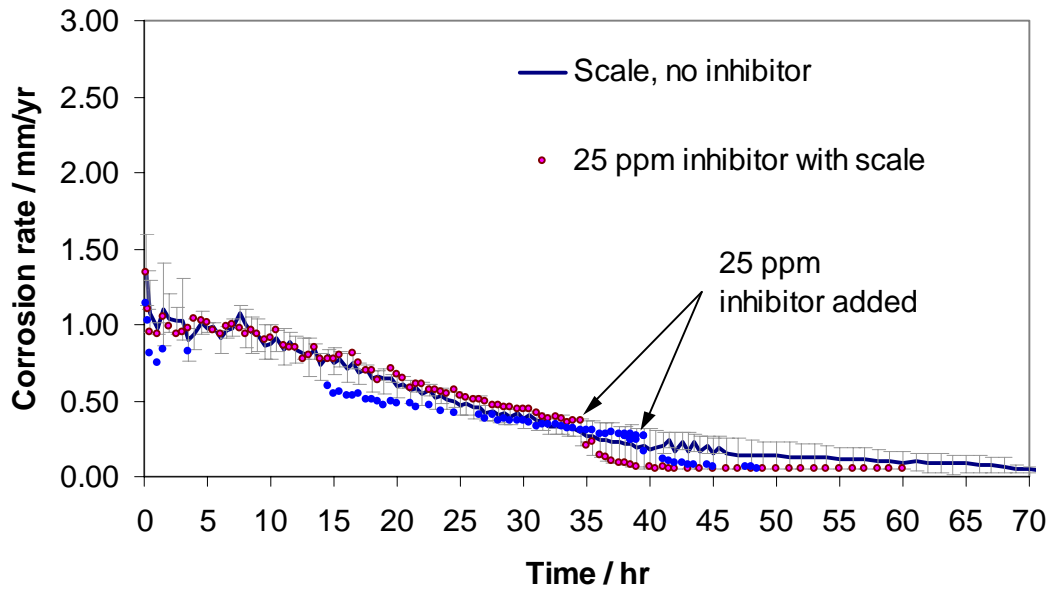


Figure 20. Effect of addition of 25 ppm inhibitor B added after 35 hr. on corrosion rate for pH 6.60, $\text{Fe}^{++} = 10$ ppm, SS = 30, $T = 80$ °C, stagnant conditions. Same symbol shapes depict repetitions of the same experiments. Error bars represent minimum and maximum values obtained in repeated experiments.

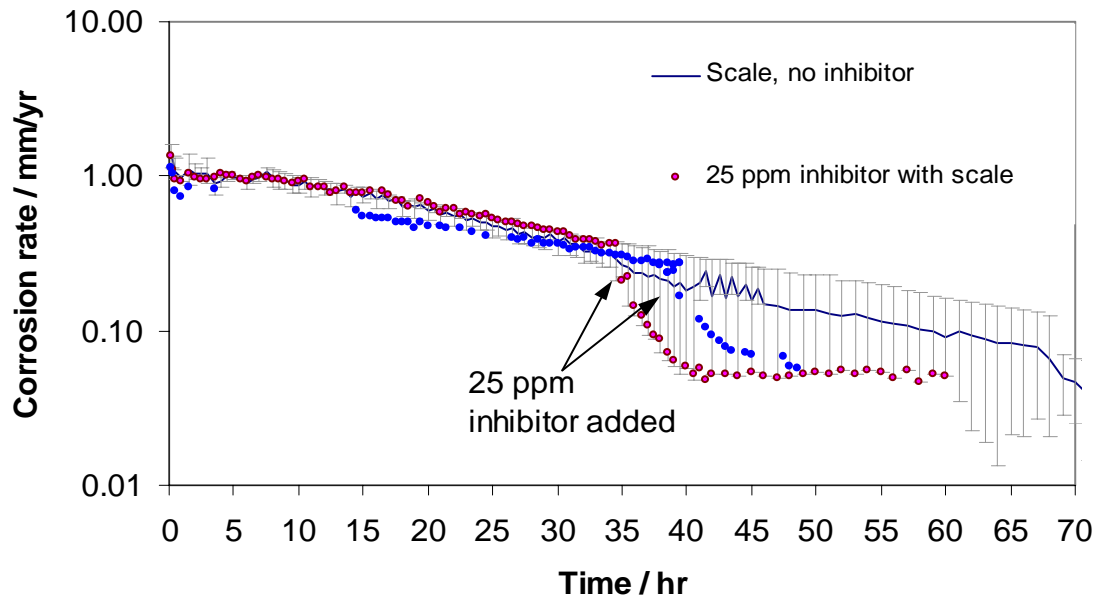


Figure 21. Effect of addition of 25 ppm inhibitor B added after 35 hr. on corrosion rate for pH 6.60, $\text{Fe}^{++} = 10$ ppm, SS = 30, $T = 80$ °C, stagnant conditions. Same symbol shapes depict repetitions of the same experiments. (For an SEM image of a coupon used in this experiment see Figure 22.)

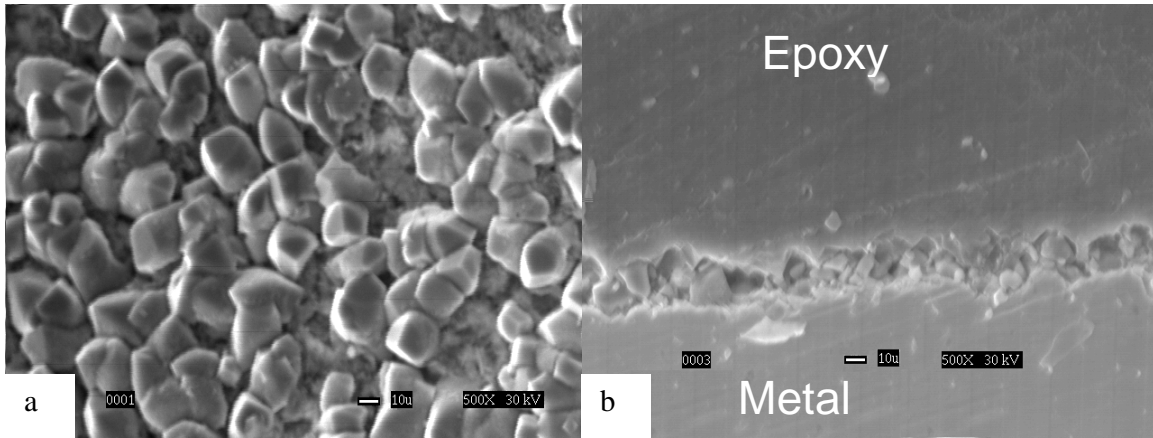


Figure 22. The top view (a) and the cross-sectional view (b) of sample at 500X when 25 ppm inhibitor B is added after 35 hr for pH 6.60, $Fe^{++} = 10$ ppm, SS = 30, T = 80 °C, stagnant conditions. (For the corrosion rate see Figure 21.)

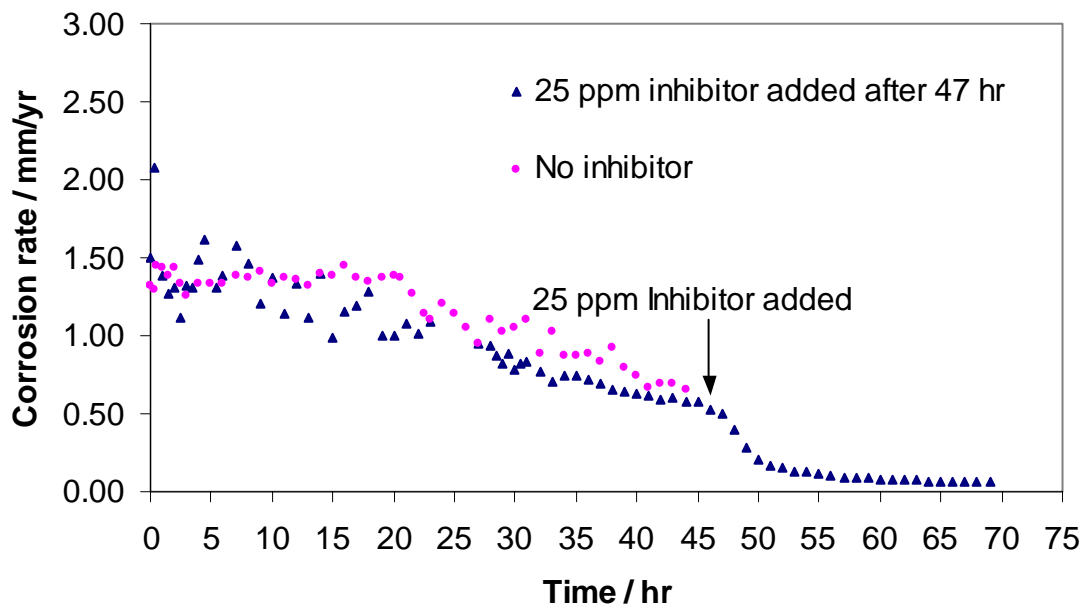


Figure 23. Change in corrosion rate with time when inhibitor B is added after 47 hours, at pH 6.30, $Fe^{++} = 10$ ppm, SS = 7, T = 80 °C, stagnant conditions. (For an SEM image of a coupon used in this experiment see Figure 24.)

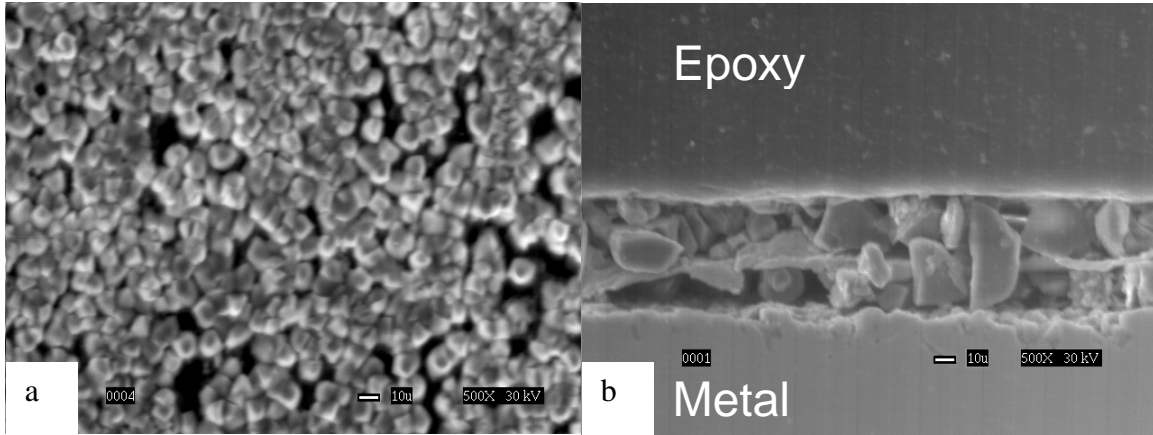


Figure 24. The top view (a) and the cross-sectional view (b) of sample at 500X when 25 ppm inhibitor B is added after 47 hr. for pH 6.30, $Fe^{++} = 10$ ppm, SS = 7, T = 80 °C, stagnant conditions. (For the corrosion rate see Figure 23.)

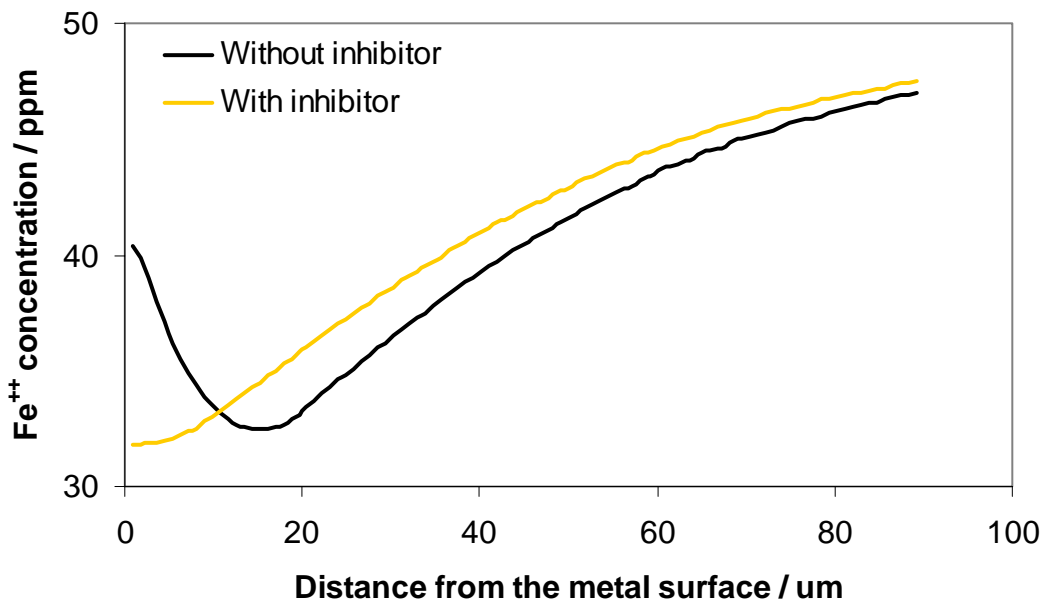


Figure 25. Fe^{++} concentration profile with and without the inhibitor obtained using the OU model at pH 6.60, $Fe^{++} = 50$ ppm, SS = 150, T = 80 °C.

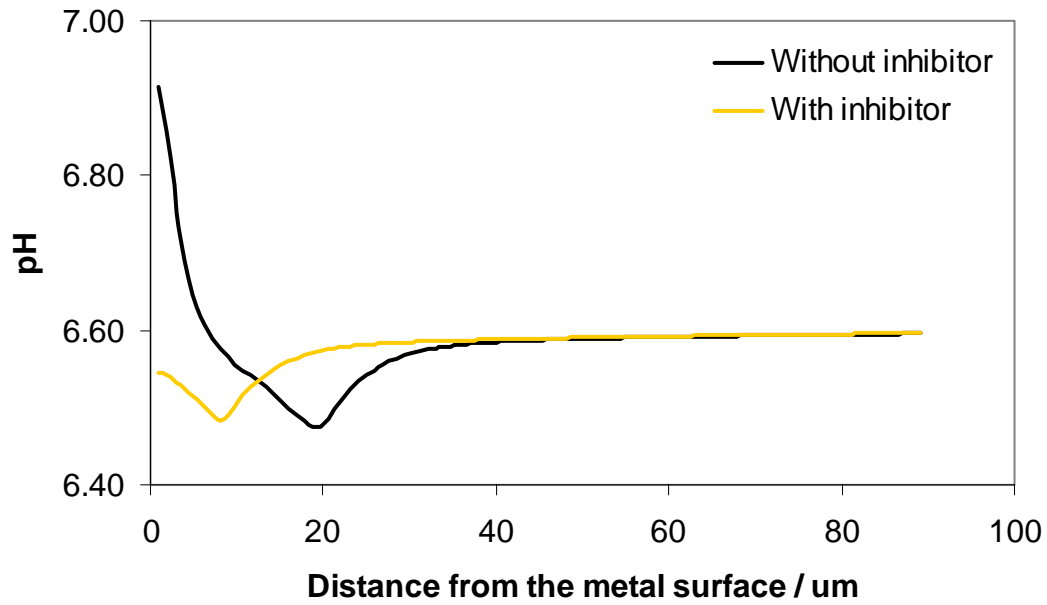


Figure 26. pH profile with and without the inhibitor obtained using the OU model at pH 6.60, $Fe^{++} = 50$ ppm, SS = 150, T = 80 °C.

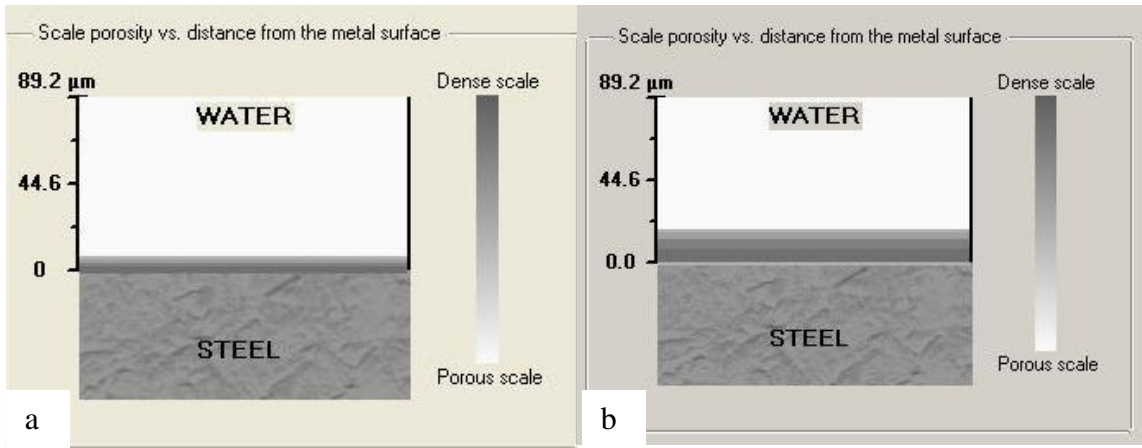


Figure 27. Comparison of the iron carbonate scale obtained (a) with and (b) without inhibitor using the OU model at pH 6.60, $Fe^{++} = 50$ ppm, T = 80 °C.